Electronic structure of $La_{1-x}Ca_xMnO_3$ determined by spin-polarized x-ray absorption spectroscopy: Comparison of experiments with band-structure computations

Q. Qian,[1] T. A. Tyson,[1] S. Savrassov,[1] C.-C. Kao,[2] and M. Croft[3]
[1]*Department of Physics, New Jersey Institute of Technology, Newark, New Jersey 07102, USA*
[2]*Brookhaven National Laboratory, Upton, New York 11973, USA*
[3]*Department of Physics and Astronomy, Rutgers University, Piscataway, New Jersey 08854, USA*
(Received 11 December 2002; revised manuscript received 24 March 2003; published 25 July 2003)

A model was developed to predict the temperature dependent changes in the local magnetic ordering based on spin-polarized Mn *K*-edge measurements of $La_{1-x}Ca_xMnO_3$. With this model, one can ascertain the change in local ordering that occurs on transiting the magnetic ordering temperature. Parallel local density approximation (LDA) and LDA+U computations are used to label the symmetries of the unoccupied bands, determine the degree of electron correlation and to provide a direct comparison with the band ordering predicted by the temperature dependent spin-polarized measurements. The spin magnetic moment and ordering of the t_{2g} and e_g states are also determined. We find that the occupied t_{2g} orbitals are always ordered with lobes near 45° to the local Mn-O directions. The Mn *K*-edge main line splitting is discussed in terms of the effective spin-polarized charge density. The oxygen hole contribution to the net magnetic moment is seen to be important. We survey the spin-polarized x-ray absorption near-edge spectra of a large group of manganese oxides and show the general trends in the main line spin splitting as a function of valence.

DOI: 10.1103/PhysRevB.68.014429 PACS number(s): 75.47.Gk, 78.70.Dm, 75.25.+z, 71.20.−b

I. INTRODUCTION

Mn *K*-edge x-ray absorption spectra (XAS) and x-ray emission spectra have been shown to be valuable in probing the valence and local structure about the Mn sites in manganites.[1–4] Recently, changes have been observed in the pre-edge spectra with temperature on crossing a magnetic ordering temperature.[5,6] In addition, a connection between Mn *K*-edge pre-edge spectra and the Mn 3d band was noted in band structure computations by Elfimov *et al.*[7] Building on this previous work, we recently developed a model that connects these changes in temperature with change in the local magnetic ordering.[8]

Spin-polarized x-ray absorption near edge spectroscopy (SPXANES) gives a direct approach to resolve the spin dependence of x-ray absorption near-edge spectral (XANES) features. This approach is based on energy resolving the 3p to 1s transition (K_β emission) and measuring the emission from the main or satellite lines as a function of incident x-ray energy. The first measurements were performed by Hämäläinen *et al.*[9] on MnO and MnF_2. Although the statistics were not ideal, these experiments paved the way to measure open-shell 3d elements systems.[6,9–12]

In this work we expand on the model presented in our previous letter[8] on $La_{1-x}Ca_xMnO_3$ by including additional doping samples ($x=0.7$) and the details of the main edge spin splitting. The change in magnetic ordering across the entire doping range is thus illustrated and discussed in terms of our transition model (Sec. III A). To complete this work, we performed comparative band structure computations (Sec. III B). Using these results we confirm that the pre-edge can be used to predict changes in the local magnetic ordering in the manganites. In addition, comparison of the experimental results with bandstructure models gives insight on the occupancies of the bands in these highly covalent materials. The importance of the oxygen hole contribution to the magnetic moment is seen both in the experimental results and the bandstructure computations.

II. EXPERIMENTAL AND COMPUTATIONAL METHODS

Samples of $La_{1-x}Ca_xMnO_3$ were prepared as described in Ref. 1. Measurement samples were prepared by finely grinding the materials and brushing the powder onto adhesive tape.

The Mn SPXANES measurements were performed at the National Synchrotron Light Source's (NSLS) 27-pole wiggler beamline X21A. Data were collected by monitoring the K_β fluorescence yield at two energies [specific to spin up (the satellite line[6,24]) and spin down (0.5 eV above the main emission line for each Mn valence)] while the incident energy was scanned across the near edge region. Measurements were performed for $x=0$, 0.3, 0.5, and 1 at 15 and 300 K. Spectra for $x=0.7$ and additional Mn systems were recorded only at 300 K. Fluorescent backgrounds and Raman effects were removed[10] and the spectra were normalized to unit area.

To access the importance of correlational effects for Mn 3d electrons, we used both local density approximation (LDA) and LDA+U methods[13] in our electronic structure computations. The latter is seen as a static limit of the dynamical mean field approach[14] and has been found to work well for many systems.[15] We use the on-site Coulomb parameter $U=6$ eV and exchange parameter $J=0.88$ eV in our calculations as implemented in the previous studies.[7,16] A full potential linear muffin-tin orbital (FP-LMTO) method of Ref. 17 is used in solving the Kohn-Sham equations where

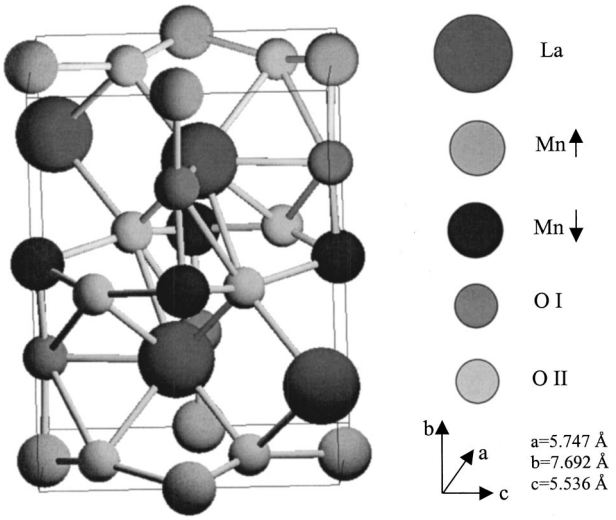

FIG. 1. The distorted *Pnma* crystal structure of $LaMnO_3$, giving the cell used in the LDA/LDA+U calculations which contains four units of $LaMnO_3$. In decreasing sphere size the La, Mn, and O atoms are shown as illustrations.

no shape approximations are made either for the charge density or the potential. All relevant quantities are expanded as spherical harmonics inside muffin-tin spheres and as plane waves in the interstitial region. Crystal structural data corresponding to four formula units (20 atoms) with antiferromagnetic spin alignment were taken from Refs. 18 and 19 for $LaMnO_3$ [*A*-type antiferromagnetic (AF)] and $CaMnO_3$ (*G*-type AF), respectively. A diagram of the structure of $LaMnO_3$ is given in Fig. 1. The muffin-tin sphere radii were $R_{La}=2.879$ a.u., $R_{Mn}=2.016$ a.u., $R_{O1}=1.702$ a.u., and $R_{O2}=1.584$ a.u., and the 1 kappa LMTO basis includes $4s$, $4p$, and $4d$ orbitals at the La site, $3s$, $3p$, and $3d$ orbitals at the Mn site and $2s$ and $2p$ orbitals at the O site with tail energy $K^2=-0.1$ Rv. Note that for the projected density of states our coordinate system was rotated by 45° about the *b* axis, as done by Elimov *et al.*[7]

The computations for the Mn K_β fluorescence spectra [Fig. 2(b)] are based on atomic and crystal field theories. In this model, we take account of the effective exchange splitting as well as all possible couplings of the angular moment (orbital and spin) of all electrons outside of closed shells or holes in filled shells. Additional energy splittings from a cubic crystal field and from $3d$ spin-orbit coupling are also considered in our calculation. Similar calculation methods have been reported by Peng *et al.*,[20] Wang *et al.*,[21] and de Groot *et al.*[22] The parameters used in the calculation are the $3p$-$3d$ and $3d$-$3d$ Slater integrals, and the $3p$ as well as $3d$ spin-orbit couplings. The atomic values for Slater integrals were obtained from Hartree-Fock computations. These values were scaled by a factor of 60% to account for the effects of covalency.[2] The calculated spectral lines were convoluted with a Lorentzian which reflects lifetime broadening and with a Gaussian which accounts for experimental broadening. Absolute energy positions cannot be obtained from these calculations.

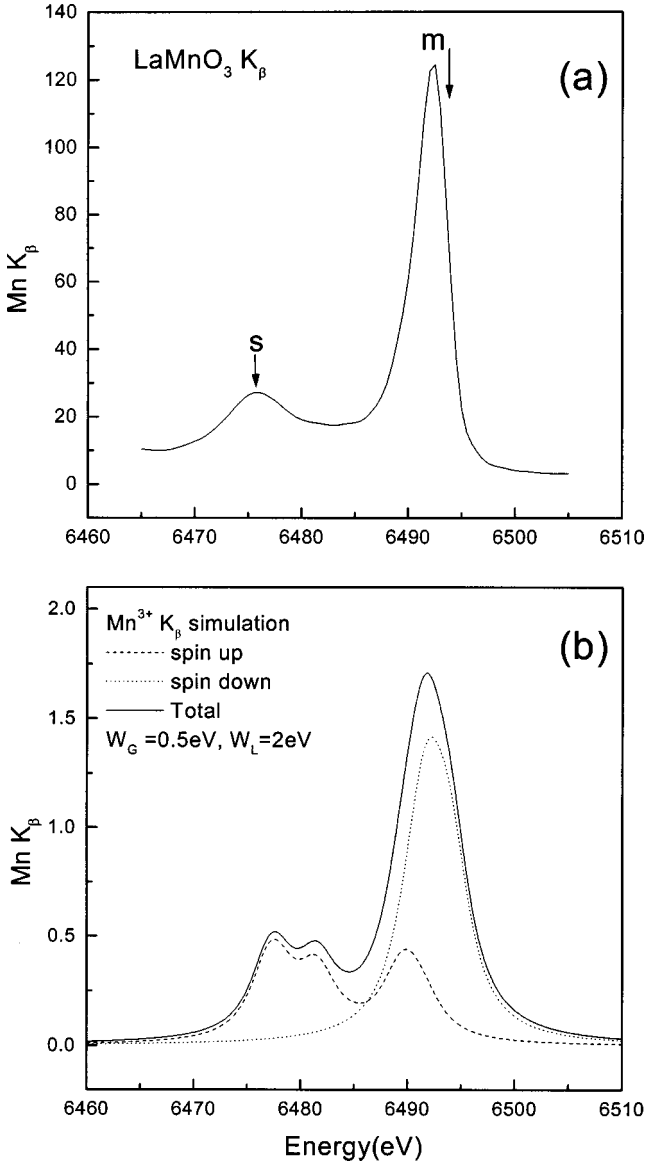

FIG. 2. (a) The measured $LaMnO_3$ K_β emission spectrum and (b) its simulation from a crystal field multiplet calculation. A Lorenz broadening of 2 eV is included and an experimental Gaussian width of 0.5 eV was also incorporated.

III. EXPERIMENTAL RESULTS

A. X-ray emission measurements

1. Introduction to K_β x-ray emission spectroscopy

To address the spectral shape of the Mn K_β emission spectra presented here, consider the photoionization excitation of a Mn atom in a solid by a x-ray photon. Since dipole photoexcitation is spin invariant, the creation of a core hole of spin-up or spin-down symmetry (relative to the total $3d$-band spin) are equally likely. In the $3p\rightarrow 1s$ decay process (K_β emission), the coupling between the $3p$ hole (or $3p$ electron spin now left unpaired) and the $3d$ electrons produce two possible final states of different energies. One observes (in Mn^{3+} for example) differences in the energy of the coupled spin-down $3p$ hole $[\Psi(3p(\uparrow)3d^4)]$ state and

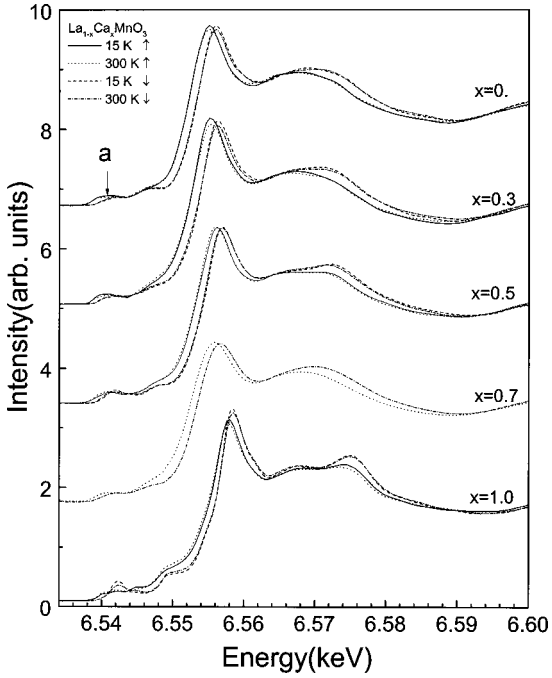

FIG. 3. Spin and temperature dependent XANES spectra of $La_{1-x}Ca_xMnO_3$. The solid line corresponds to a spin-up electron excited from the 1*s* state measured at 15 K while the dotted line is used for the 300-K spin-up spectrum. The dashed line corresponds to spin-down electrons excited from 1*s* at 15 K, while the dash-dotted line is used for the 300-K spin-down channel.

spin-up hole state ($\Psi(3p(\downarrow)3d^4)$. For a fixed incident photon energy $\hbar\omega$ above the Mn *K* edge, the K_β emission spectrum of photons $\hbar\Omega$ can be resolved into these two components- a main line (m) and a satellite line (s) [Fig. 2(a)]. Qualitatively, it is found that the energy splitting between the main line and satellite is given by $\Delta E_{sm}=J(2S+1)$, while the intensity ratio of the satellite to the main peak is given by $I_s/I_m=S/(S+1)$, where S is the total spin of the unpaired electrons in the 3*d* shell and J is the exchange integral.[23]

Figure 2(b) gives a simulation for an Mn^{3+} ion (such as Mn in $LaMnO_3$). From the measurement [Fig. 2(a)] and the simulation, we can see clearly that the spin-up and spin-down lines are well separated. The sum gives excellent agreement with the experiment spectrum in Fig. 2(a). The *K*-edge SPXANES were obtained by focusing the analyzer on these two different channels (emission energies) separately and then scanning the incident x-ray energy across the *K* edge. The arrows in Fig. 2(a) show the monitor points-one set on the high energy shoulder on the main peak to avoid the tail of the spin up channel.

2. Observed temperature dependent K-edge SPXANES in $La_{1-x}Ca_xMnO_3$

Figure 3 shows the temperature dependence of the full *K*-edge SPXANES of $La_{1-x}Ca_xMnO_3$. A clear splitting between the spin up and spin down channels is seen. The exchange interaction of the photoelectron with the spin up and spin down densities of states due to the unpaired spin on the Mn sites (3*d* electrons) produces this splitting. Both regions are expanded in Fig. 4.

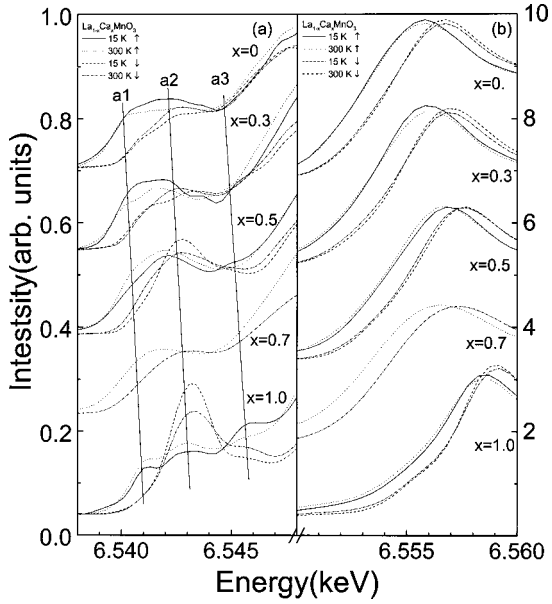

FIG. 4. (a) The expansion of the pre-edge region feature *a* of Fig. 3. The three straight lines indicate the *a*1, *a*2, and *a*3 features. (b) The expansion of the main edge region of Fig. 3 is shown.

Figure 4(a) gives the pre-edge region (labeled *a* in Fig. 3) of the SPXANES spectra. Significant temperature and spin dependence of the pre-edge spectra are seen. Due to quite low 1*s* to 3*d* quadrupole transition intensities,[24] the pre-edge features are expected to have other origins. In our previous work,[8] we developed a model in which these feature are primarily from on site Mn 4*p* overlap with neighboring Mn 3*d*. In that simple physical picture, the Mn 1*s* electron can undergo a transition to final states formed by this hybridization and the intensity are sensitive to the local magnetic ordering.

The connection of the pre-edge region of Mn *K*-edge spectrum and the *d* density of states was put on a solid foundation by the LDA+*U* band structure calculations of Elfimov *et al.*[7] In this work, they computed the partial Mn 3*d* partial density of states (DOS) and showed that in the low energy region of the 4*p* partial DOS there was a feature that had the same spin polarization, occurred in the same energy range and had the same distribution as the Mn 3*d* partial DOS. Further embedded cluster computations have shown explicitly that the pre-edge feature is the result of a transition from 1*s* to a 4*p* state hybridized with the neighboring Mn 3*d* state.[25]

In our model, we make the further assumption that the 1*s* to t_{2g} transition intensity vanishes. Since the system, $La_{1-x}Ca_xMnO_3$, exhibits orbital ordering over a broad range of x,[26] the e_g ($d_{x^2-r^2}$,$d_{y^2-z^2}$) always align along Mn—O bond directions while the t_{2g} orbitals (d_{xy}, d_{xz}, d_{yz}) are off axis. As seen below, the theoretical map of the spin density supports this assumption. This means that the t_{2g} orbitals can not contribute to the pre-edge feature. Indeed both embedded cluster calculations[25] and LDA calculations[27] predict no t_{2g}

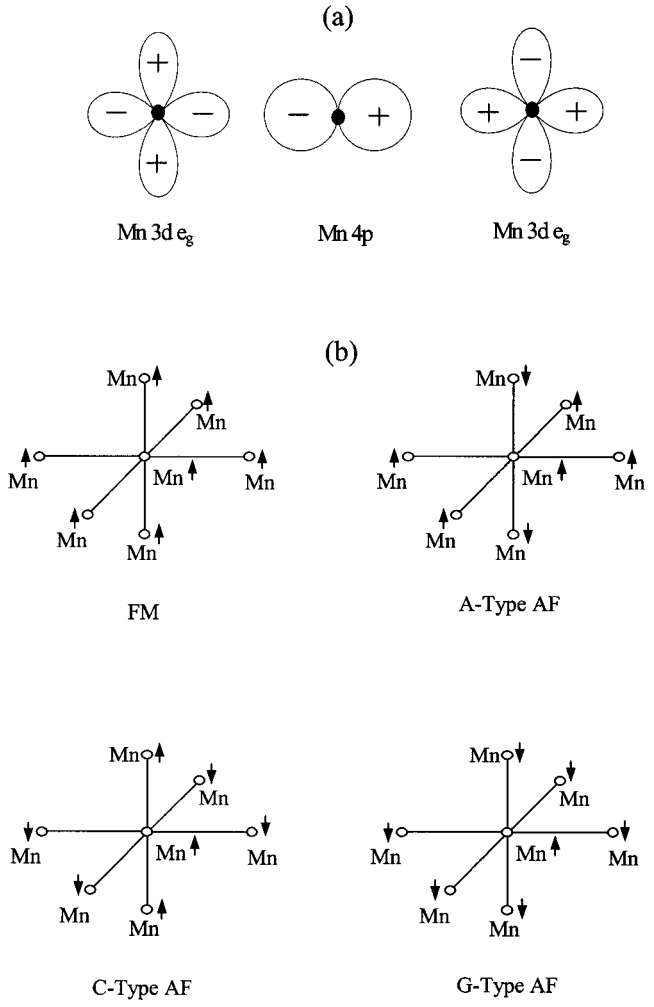

FIG. 5. (a) A model for Mn $4p$ hybridized with neighboring Mn $3d$ e_g orbitals. (b) Local view of Mn majority spin arrangements for four magnetic orderings (FM, *A*-AF, *C*-AF, and *G*-AF) in a $La_{1-x}Ca_xMnO_3$ system below T_c or T_N. The arrows show each Mn majority spin direction. The O atoms have been left out for clarity.

contribution to the Mn *K*-edge XAS. LDA computations predict orbital ordering even in the $CaMnO_3$ end member.[28] This will be seen more clearly in band structure computations (Fig. 12).

3. Proposed transition model of magnetic ordering

We now expand on the description of model developed in our previous paper,[8] which is based on these assumptions, which followed the rule of spin conservation (without t_{2g} final states). To explain the pre-edge feature, we start with $LaMnO_3$ which is an *A*-type antiferromagnet (AF) (see Refs. 29 and 30 for magnetic ordering) below $T_N \sim 130$ K.[26] Below T_N, each Mn ion is surrounded by four Mn ions (through the oxygen) with majority spin parallel and two Mn atoms with majority spin anti-parallel to the central Mn majority spin, as shown in Fig. 5(b). Above T_N, each Mn has six Mn neighbors with randomly distributed majority spin direction.

Before moving to a discussion of the details of the pre-edge transitions we point out the ordering of the *d* levels.[31]

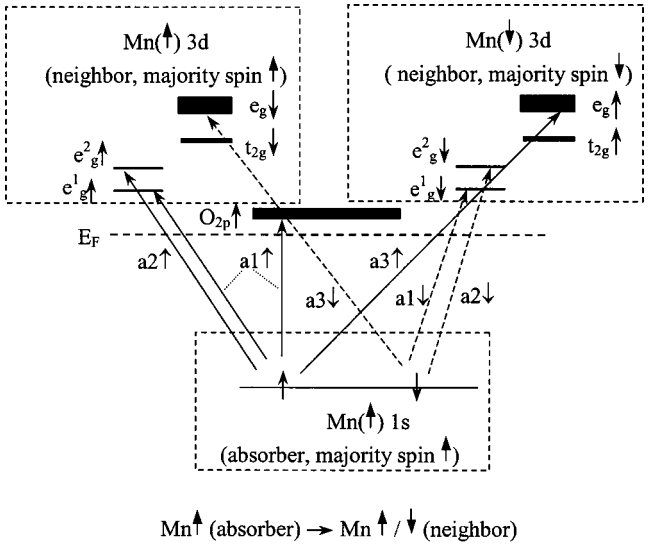

FIG. 6. A schematic diagram showing the transitions in the pre-edge for spin polarized absorption in the magnetically ordered state of *A*-type AF $LaMnO_3$. It shows two possible neighbor transitions due to $4p$-$3d$ hybridization which allow transitions to the *d* final state of a neighbor in same spin polarization as the absorber (upper left) as well as the case where the spin polarizations are reverse (upper right).

Considering the spin-up channel, the fivefold degenerate atomic $3d(\uparrow)$ states are split into $t_{2g}(\uparrow)$ and $e_g(\uparrow)$ states by the octahedral symmetry crystal field—with the t_{2g} states occurring at lower energy. Furthermore, the Mn^{3+} ion ($LaMnO_3$) with a single electron in the $e_g(\uparrow)$ state undergoes a Jahn-Teller distortion splitting the $e_g(\uparrow)$ levels. The $e_g(\uparrow)$ and $t_{2g}(\uparrow)$ are further broadened into bands by combining the atoms to form a solid. Consequently, the first completely empty *d* state will be an $e_g(\uparrow)$ state. This state will be followed by $t_{2g}(\downarrow)$ and $e_g(\downarrow)$ states. LDA+*U* band structure computations below show that O $2p(\uparrow)$ states occur near the $e_g(\uparrow)$ bands. These ideas are used to construct the transition diagram for the pre-edge features.

Figure 6 shows the transition model for pre-edge feature, which is based on dipole transitions (Mn $4p$ hybridized with neighbor Mn e_g). Three boxes are defined by dashed lines, the central absorbing Mn site is represented as the lower one, defined as majority spin-up (↑). The upper left box corresponds to a neighboring Mn site with majority spin-up (↑). We marked the upper right box as a neighboring Mn site with majority spin-down (↓) since its spin is antiparallel to absorber's. Here, we assume that the energy levels are the same for both neighbors. From the lower box, Mn $1s(\uparrow)$ an electron can make a transition to an $e_g(\uparrow)$ orbital of the neighbor Mn(↑) (in left upper box) with the same spin alignment, (density of states computations shown below reveal holes in the majority e_g^1 band due to covalency), and also it can be excited to a local minority spin orbitals $e_g(\uparrow)$ of the neighboring Mn(↓) (in right upper box) according to spin conversation. Notice in the case of the Mn(↓) neighbor, the local majority spin e_g orbital is labeled as $e_g(\downarrow)$, as shown in the right upper box in Fig. 6. Evidence of O $2p$ holes in $LaMnO_3$ was found in optical measurements by Ju *et al.*[32] as

well as in our LDA calculation. That is why we need to include O $2p$ spin-up channel transition in Fig. 6, in which, O $2p$ is hybridized with the Mn $4p$ states. This assumption also matched our pre-edge feature for later discussion. In Fig. 6, note that the labels $a1$, $a2$, and $a3$ refer to pre-edge a features in Fig. 4(a), long solid arrows correspond to the spin-up transition channels, while dashed ones give the spin-down transition channels.

4. Application of the transition model of magnetic ordering to $La_{1-x}Ca_xMnO_3$

Now let us turn to the temperature dependence of our pre-edge SPXANES. For comparison with bandstructure computations and to illustrate the use of the model, we give a more complete discussion and cover a broader range of samples.

$LaMnO_3$ is an *A*-type AF at 15 K, and is paramagnetic at 300 K. On crossing T_N, from low temperature to high temperature, the Mn majority spins alignment will change to a random distribution-meaning that the number of ferromagnetically aligned Mn neighbors changes from four to an average of three. This must enhance the transitions in the antiparallel channel shown in Fig. 6 (upper right) and reduce those in parallel channel of Fig. 6 (upper left). Then, the $a1$ and $a2$ intensities should decrease, while the $a3$ intensity should increase in the spin-up absorption channel, where the level of the locally spin down e_g minority is higher than that of the spin-up majority (see theoretical calculations below). The temperature dependence of the spin down channel is expected to be reversed since the process is reversed. This is exactly what we had seen in Fig. 4(a), despite the broadness of the $a3$ feature in high background. Note there is a shift between the spin up and spin down spectra in all pre-edge spectra. This shift may come from the difference between the $1s$ excitation energies for spin up and spin down. From our calculations below, the large $a1$ feature for $x=0$ in the spin up channel is due to transitions to O $2p$ (near the Fermi energy). The suppression of the temperature difference in the spin up $a1$ region is due to an increase in holes on the O $2p$ band due to increased covalency at low temperature.[6]

For $x=0.3$, the system is ferromagnetic at low temperature [$T_C \sim 250$ K (Ref. 26)]. It is expected to have similar trends to the parent $LaMnO_3$ which is locally partially ferromagnetic (four spins up and two down with respect to the central Mn site) at low temperature. But due to its metallic property, there is delocalization (e_g^1 becomes accessible for transition) of the majority spin e_g^1 electron (seen as an increase in conductivity)—the $a1$ feature increases at low temperature. Also, an increase of O $2p$ holes due to increased covalency at low temperature[6] further enhances this $a1$ feature. For the spin down channel, $a1$ and $a2$ features are expected to decrease at low temperature. However, no strong reduction is seen. This observation is not easy to reconcile with the results of neutron diffraction refinements. But diffraction provides a picture of the long range ferromagnetic ordering, while our measurements give a local picture. These spin down intensity features at low temperature which are due to antiparallel neighbors existing below T_c possibly due to the FM and AF phase separation suggested initially by Wollan and Koehler[33] and more recently by Moreo *et al.*[34]

In $x=0.5$ system at low temperature, each Mn ion has four neighboring Mn ions with antiparallel spin and two neighbors with parallel spin exhibits. It belongs to *C*-type AF order [below $T_N \sim 150$ K (Ref. 26)]. From our model, it is expected that the temperature dependence should be reversed compared to the $x=0$ system. At low temperature [below $T_{co} \sim 150$ K$=T_N$ (Ref. 26)], O $2p$ holes are delocalized due to reduced covalency at low temperature.[6] On the other hand, the majority spin e_g^1 electrons are localized as seen from the observed increase in resistivity at low temperature.[35] Hence, at low temperature, the $a1$ feature is reduced as observed in accordance with our model. The similarity of the 300-K spectra of the $x=0.5$ and 0.7 systems are due to the equivalent random ordering of the Mn moments.

The end member system $CaMnO_3$ is thought to be a *G*-type AF at low temperature [$T_N \sim 125$ K (Ref. 26)], where each Mn ion has six antiparallel Mn neighbors. The large $a1$ spin up peak is from transitions to unoccupied O $2p(\uparrow)$ states. Ferromagnetic ordering of $CaMnO_3$ produces a split O $2p$ band near the Fermi level which will be shown below. It is possible that $CaMnO_3$ is a two-phase material composed of FM and *G*-AF (domains) regions. Indeed it is known that $CaMnO_3$ has a small net magnetization,[36] which has previously been attributed to defects. In the $a1$ peak at 15 K the low intensity is due to a reduction in the covalency of $CaMnO_3$ below T_N.[6] No transition to O $2p(\downarrow)$ is observed in the $a1$ region in spin down spectra consistent with our band structure calculation (which shows no O $2p(\downarrow)$ density just above Fermi level). The low temperature $a2$ peak in the spin up spectrum can be explained as the result of Mn sites within the FM ordered regions (discussed above). The temperature dependent behavior of $CaMnO_3$ with the exception of the $a1$ feature is expected to be similar to that of $x=0.5$ system and this is what is observed.

B. Comparison of experimental SPXANES with LDA/LDA+*U* band structure computations

1. Band structure computations

Figure 7 presents the LDA$+U$ and LDA density of states calculations for Mn $3d$ band of $LaMnO_3$. In the top panel the orbitals, spin up e_{g1}, and e_{g2} all have intensity above E_f. Hence the spin up e_{g1} is not full occupied—unexpected for an ionic system. Note that the spin down e_g orbitals are 5–6 eV higher than the spin up orbitals. We also list the t_{2g} states in panel (b), and total $3d$ band for the LDA$+U$ and LDA in panels (c) and (d), respectively, for comparison. It is clear that the on site Coulomb interaction U makes the spin up and spin down band splitting much larger. By comparison, no unoccupied band occurs 4 eV above E_f in the LDA computation. In addition, the gap at E_f is significantly reduced in the LDA computation. The consistency of the LDA$+U$ with the strong insulating behavior of the materials shows that $LaMnO_3$ is highly correlated. In Fig. 8 we show the LDA$+U$ and LDA calculation for type-II O $2p$ (in the *a*-*c* plane) partial DOS. We see that in Fig. 8(a) there is a

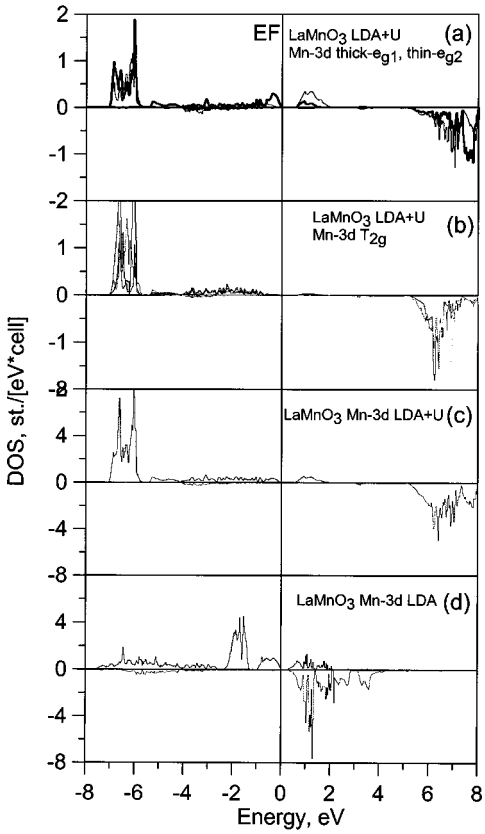

FIG. 7. LDA+U and LDA partial DOS's of Mn $3d$ in $LaMnO_3$. For a given set of states, the upper panels refer to the majority spin and the lower half refer to the minority spin. In (a) we give the Mn $3d$ e_g orbitals. The thick line is for the e_{g1} state while the thin line gives the e_{g2} state. In (b) we give the Mn $3d$ t_{2g} orbitals while in (c) and (d) we show the total LDA+U Mn $3d$ band and LDA Mn $3d$ band, respectively.

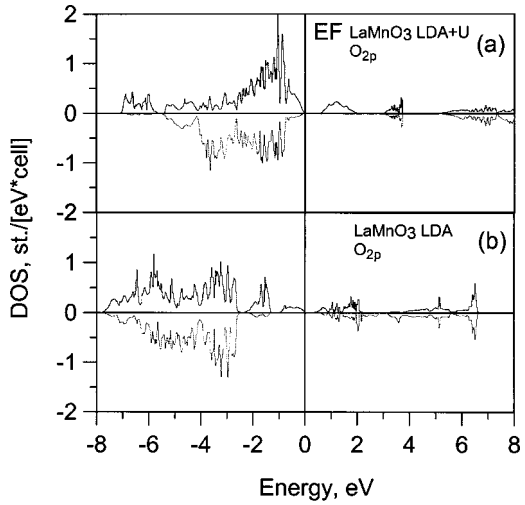

FIG. 8. Type-II O $2p$ DOS of $LaMnO_3$ for (a) LDA+U and (b) LDA calculations. The upper half is for majority spin states and the lower half is for minority spin states.

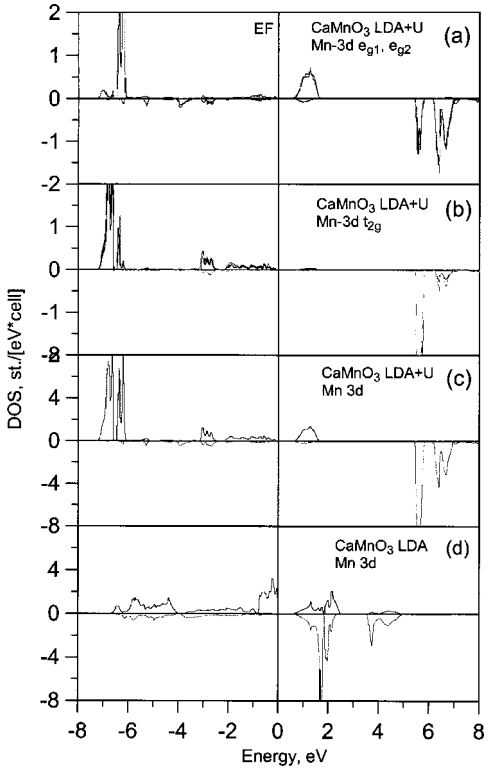

FIG. 9. Partial DOS of LDA+U and LDA calculations for Mn $3d$ of $CaMnO_3$. (a) Note that there is no difference between the e_{g1} and e_{g2} orbitals due to the absence of a Jahn-Teller distortion. In (b) we give the Mn $3d$ t_{2g} orbitals, while in (c) and (d) we show the total LDA+U Mn $3d$ band and LDA Mn $3d$ band, respectively.

spin-up density 1–2 eV above E_f in LDA+U, but no spin down density in this range. These results agree with our model in which we observe transitions to the spin-up O $2p$ channel but not to the spin down channel. In the LDA calculation in Fig. 8(b), there are both spin up and spin down intensity at 1–2 eV above E_f, which disagrees with our experimental results on $LaMnO_3$. We note that the type-II O is spin polarized and has a net magnetic moment due to the fact that, unlike O I on the b axis, the Mn-O-Mn chain is not symmetric (both Mn—O bonds are not equal).

In Fig. 9, we show the LDA+U and LDA calculations for G-type $CaMnO_3$. The difference between the LDA+U and LDA calculations is the spin up and spin down splitting. In the LDA computation, the e_g spin-down state is only 2.5 eV above the e_g spin-up states, which agree with $a2$-$a3$ splitting in Fig. 4. Figure 10 gives the LDA+U results of the type-II O $2p$ DOS of G-AF type $CaMnO_3$. It is seen that there is density both in the spin up and spin down states just above E_f. This means that in G-AF there is no spin polarization of the O $2p$ band. This is inconsistent with our model interpretation above, which shows intensity only in the spin up channel for the $a1$ feature. Hence, one must consider the possibility of local FM ordering in $CaMnO_3$. In Fig. 11, which gives results for FM ordered $CaMnO_3$ in the LDA +U approximation, we can see the spin-up intensity in the type-II O $2p$ just above E_f, but not in the spin-down state. Based on our discussion, we think that $CaMnO_3$ is a G-type

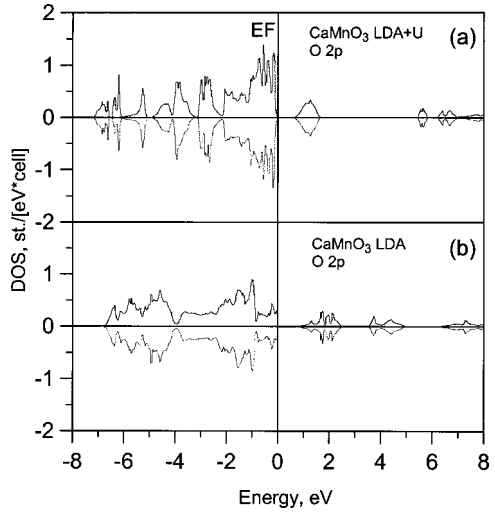

FIG. 10. Type-II O $2p$ DOS of $CaMnO_3$ for (a) LDA+U and (b) LDA calculations. The upper half is for majority spin states and the lower half is for minority spin states. Notice the symmetry (equivalence) of the high spin and low spin distribution at an energy 1 eV above Fermi level.

AF mixed with a small component of FM ordered regions—consistent with the observation of a net magnetic moment.[36] This conclusion is quite consistent with our SPXANES.

In Fig. 12 we show the net spin density (spin-up charge density minus spin down charge density) of $LaMnO_3$ and $CaMnO_3$ in the *a-c* plane (010) for AF ordering as well as for

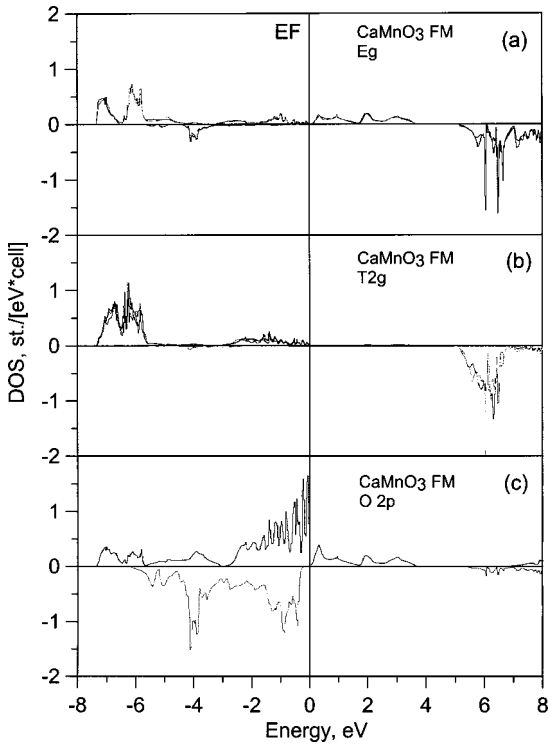

FIG. 11. DOS of FM $CaMnO_3$ for the Mn $3d$ band and type-II O $2p$ band in a LDA+U calculation. We show the (a) e_g band, (b) t_{2g} band and (c) type-II O $2p$ band. The upper half corresponds to majority spin states and the lower half to minority spin states.

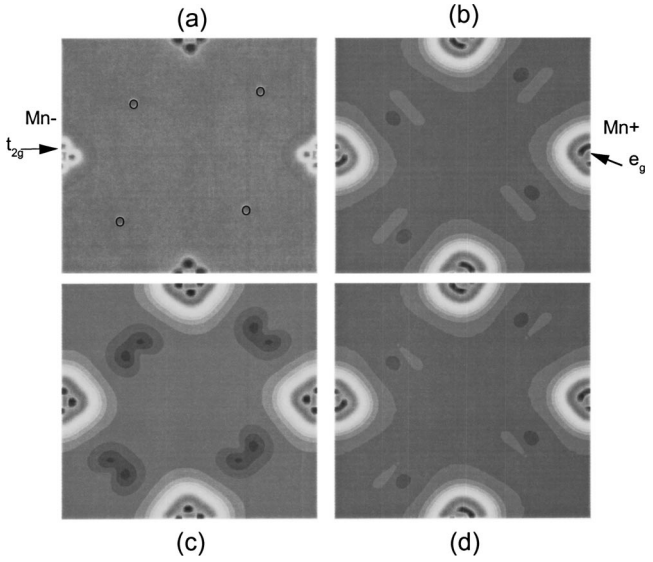

FIG. 12. The net spin density in the (010) *a-c* plane for $CaMnO_3$ and $LaMnO_3$ for LDA+U calculations. The Mn site is at the middle of each of the four edges in the panel. Oxygen atoms reside between the Mn sites. Here Mn^+ and Mn^- represent two opposite majority spin states, respectively. (a) *G*-AF $CaMnO_3$: the *o* marks O II positions, which have no spin contribution. (b) *A*-AF $LaMnO_3$, (c) FM $CaMnO_3$ and (d) FM $LaMnO_3$. Notice that there is an O II contribution between close Mn ions in panels (b), (c) and (d). Observe that in (a) we can clearly see the t_{2g} lobes at $\sim$45° to the Mn—O bonds. In (b) one can clearly see ordered e_g lobes (pointing along the Mn—O bond direction) as shaded region between the t_{2g} lobes. For all magnetic orderings the t_{2g} states are always ordered.

FM ordering. Note that in all figures there is clear t_{2g} ordering at $\sim$45° to the local Mn—O bond directions. For $LaMnO_3$ [Figs. 12(b) and 12(d)], note the net spin on the O II site between the Mn ions. In the case of $CaMnO_3$, it is observed that only in the FM case is there a net spin density on the O II site. The e_g states in $LaMnO_3$ are ordered in both the AF state and FM states. This suggests that an orbitally (e_g) ordered and insulating FM state exists for $LaMnO_3$ as in the case of $BiMnO_3$.[37] The point to note here is that in $LaMnO_3$ and possibly $La_{1-x}Ca_xMnO_3$ the net magnetic moment observed is not entirely due to the Mn site but there is a significant contribution from the O II sites. In the band-structure computation we have found a contribution of approximately $\sim 0.1\ \mu_B$ per O II site (there are two O II per Mn). We note that in a cubic lattice $LaMnO_3$ looses the ordering of the e_g electrons making possible a metallic state.

Figure 13 shows the Mn $4p$ density of states based on LDA+U and LDA calculations for $LaMnO_3$. Roughly speaking, there is not much difference in the shape of the features between these two calculations except for the absolute energy positions. But in detail, it suggests that the spatial and spin-polarized spectral splittings are a little different. The LDA+U splitting is larger than the LDA splitting. The most important feature in common is that the majority spin DOS is at lower energy ($\sim$2 eV) in comparison with the minority spin DOS due to exchange potential. In addition the DOS spatially polarized along the short bond direction has the highest energy while that polarized along the long bond

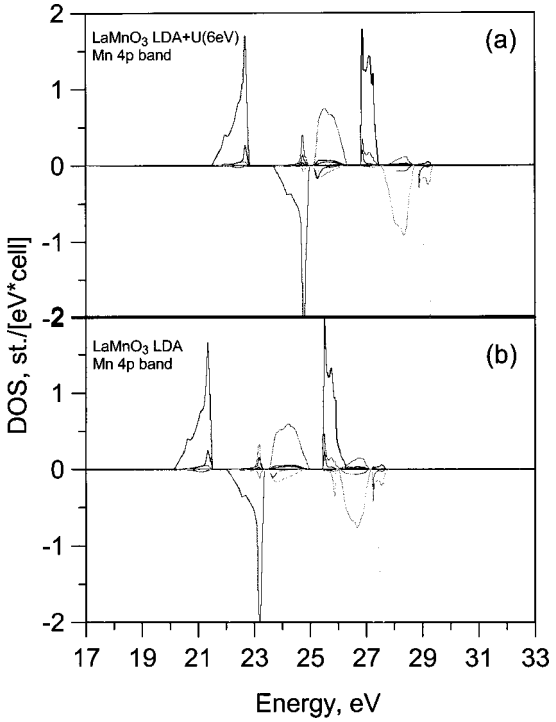

FIG. 13. Mn 4*p* DOS for (a) LDA+*U* and (b) LDA calculations. Again, the upper half gives majority spin states and lower half gives minority spin states.

direction has the lowest energy. The LDA simulations are consistent with spatially polarized XANES calculations.[38]

In Fig. 14 we show the partial DOS of the Mn 4*p* band of $CaMnO_3$ in the LDA+*U* and LDA simulations. The main result is a spin-up feature at low energy. That is consistent

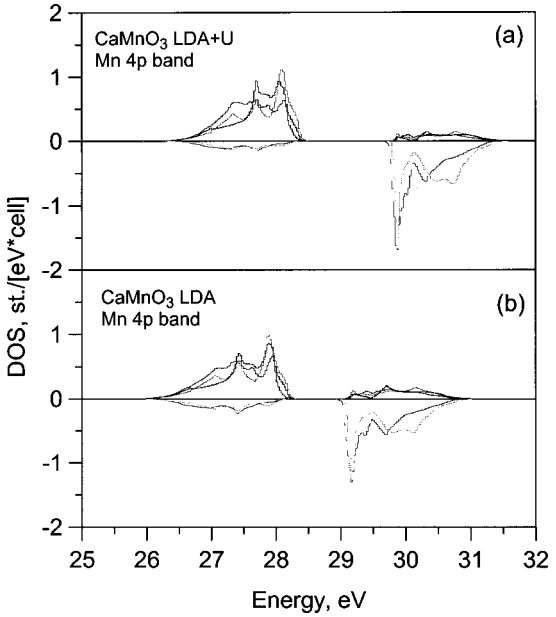

FIG. 14. Partial DOS of Mn 4*p* of $CaMnO_3$ with (a) LDA +*U* simulation and (b) LDA simulation. Notice the absence of spatial splitting in the LDA/LDA+*U* computation but large spin dependent splitting in the computations (LDA/LDA+*U*).

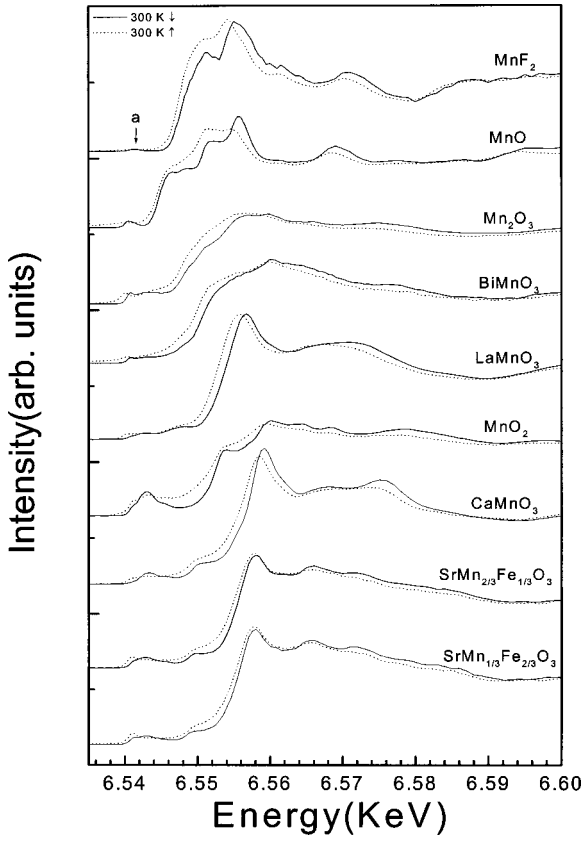

FIG. 15. Survey of SPXANES of Mn compounds at room temperature. Notice the all spectra have spin dependent main edge splitting indicating unpaired Mn 3*d* electrons. The dotted line corresponds to majority spin and solid line gives the minority spin. All spectra are area normalized.

with our SPXANES at the main edge in Fig. 4(b). Due to lower local distortion, we cannot see the spatial splitting observed for $LaMnO_3$. (We note that for $LaMnO_3$ the Mn—O bond distances in the MnO_6 octahedra[39] are 1.968, 1.907, and 2.178 Å, while for $CaMnO_3$ the values are 1.895, 1.900, and 1.903 Å.[19]) The difference between these two simulations is that LDA+*U* gives a large splitting (3 eV) between the different spin channels compared to the LDA case (2 eV). Inspecting the experimental SPXANES, we see that the LDA simulation is a little better than the LDA+*U* simulation, suggesting that $CaMnO_3$ has weaker electron correlations than $LaMnO_3$.

C. General trends in SPXANES measurements of Mn systems

We give the SPXANES spectra for a broad range of Mn systems measured at room temperature (Fig. 15) to show the general trends. The solid line is the spin-down channel and dotted line the spin-up channel. The splitting at the main edge is quite clear as we expected due to the spin dependent exchange potential in Mn systems with unpaired *d* electrons. The primary observation above the pre-edge is the spin splitting of the main line. We note that the spin-up channel has a larger Lorentz broadening than the spin-down channel,[40] and this accounts for most of the major differences in resolution in the pre-edge.

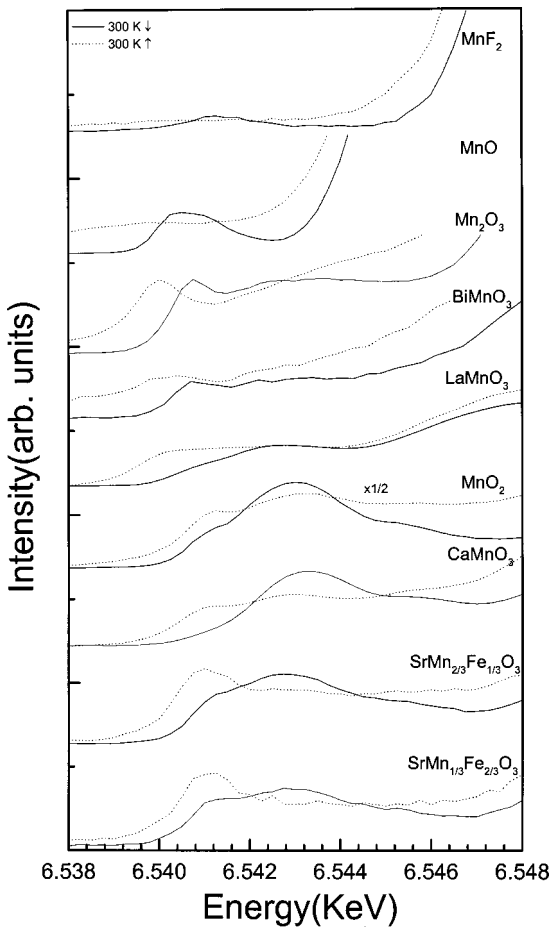

FIG. 16. Expanded pre-edge *a* feature from Fig. 15. Note the $\frac{1}{2}$ scale factor used for MnO_2. The dotted line corresponds to majority spin and the solid line to minority spin.

In Fig. 16 we expand the pre-edge region *a* of Fig. 15. It is interesting to compare the spectra of MnF_2 and MnO [both $d^5(\uparrow)$]. For the spin-down channel a large feature is seen in the pre-edge of MnO compared to a small bump in the MnF_2 spectrum. The difference between these Mn^{2+} systems is the covalency. Both systems have weak quadrupole allowed $1s$ to $3d$ transitions. But in the case of strongly covalent MnO, there are addition transitions corresponding to the $1s$ to $4p$ (with the $4p$ hybridized with the neighboring Mn e_g orbitals). These latter transitions are highly allowed in covalent systems (based on the hybridization) but are not expected in ionic systems (where only weak quadrupole transitions contribute[24]). The MnF_2 spin up pre-edge is flat [since the $3d(\uparrow)$ band is full]. The same spectrum for MnO display a broad weak feature due to $1s$ to $4p$ ($4p$ hybridized with the neighboring Mn e_g orbitals) transitions. Looking at Mn_2O_3 (Mn^{3+}) and MnO_2 (Mn^{4+}), we note that the spin-up channel becomes accessible due to the reduced $3d(\uparrow)$ occupancy, resulting progressively in larger features in this channel. The enhanced down channel intensity of the pre-edge features of MnO_2 (Mn^{4+}), compared to $CaMnO_3$ (Mn^{4+}), is mainly due to the larger covalency of MnO_2. Similar trends are seen in the Mn^{4+} systems $SrMn_{2/3}Fe_{1/3}O_3$ and $SrMn_{1/3}Fe_{2/3}O_3$.

IV. SUMMARY

A systematic study of spin dependent Mn *K*-edge x-ray absorption spectra was performed on $La_{1-x}Ca_xMnO_3$ and other Mn oxide systems. We expanded on this idea of $4p$-$3d$ overlap suggested by Elfimov *et al.*[7] and explored the details of our recently developed model of spin-polarized XANES spectra to understand the local magnetic ordering. Parallel LDA and LDA+U computations are used to label the symmetries of the unoccupied bands, to determine the degree of correlation, and to provide a direct comparison with the band ordering predicted by the temperature dependent spin-polarized measurements. The spin magnetic moment and ordering of the t_{2g} and e_g states is also determined. We find that the occupied t_{2g} orbitals are always ordered with lobes near 45° to the local Mn-O directions. The Mn *K*-edge main line splitting is discussed in terms of the effective spin-polarized charge density in the spin-up and spin-down channels. We survey the spin-polarized XANES spectra, showing the general trends in the main line spin splitting and pre-edge intensities and their relationships with covalency.

ACKNOWLEDGMENTS

Data acquisition was performed at Brookhaven National Laboratory's National Synchrotron Light Source which is funded by the U.S. Department of Energy. This work was supported by NSF Career Grant Nos. DMR-9733862 and DMR-0216858. The authors are indebted to M. Greenblatt and S.-W. Cheong of Rutgers University for sample preparation. We also thank G. A. Sawatzky of the University of British Columbia for helpful discussions.

[1] M. Croft, D. Sills, M. Greenblatt, C. Lee, S.-W. Cheong, K. V. Ramanujachary, and D. Tran, Phys. Rev. B **55**, 8726 (1997).

[2] T. A. Tyson, Q. Qian, C.-C. Kao, J.-P. Rueff, F. M. F. de Groot, M. Croft, S.-W. Cheong, M. Greenblatt, and M. A. Subramanian, Phys. Rev. B **60**, 4665 (1999).

[3] C. H. Booth, F. Bridges, G. H. Kwei, J. M. Lawrence, A. L. Cornelius, and J. J. Neumeier, Phys. Rev. B **57**, 10 440 (1998); T. A. Tyson, J. Mustre de Leon, S. D. Conradson, A. R. Bishop, J. J. Neumeier, H. Röder, and Jun Zang, *ibid.* **53**, 13 985 (1996).

[4] G. Subías, J. García, M. G. Proietti, and J. Blasco, Phys. Rev. B **56**, 8183 (1997).

[5] F. Bridges, C. H. Booth, G. H. Kwei, J. J. Neumeier, and G. A. Sawatzky, Phys. Rev. B **61**, R9237 (2000).

[6] Q. Qian, T. A. Tyson, C.-C. Kao, M. Croft, S.-W. Cheong, and M. Greenblatt, Phys. Rev. B **62**, 13472 (2000).

[7] I. S. Elfimov, V. I. Anisimov, and G. A. Sawatzky, Phys. Rev. Lett. **82**, 4264 (1999).

[8] Q. Qian, T. A. Tyson, C.-C. Kao, M. Croft, and A. Yu. Ignatov,

Appl. Phys. Lett. **80**, 3141 (2002).
[9] K. Hämäläinen, C.-C. Kao, J. B. Hastings, D. P. Siddons, L. E. Berman, V. Stojanoff, and S. P. Cramer, Phys. Rev. B **46**, 14274 (1992).
[10] F. M. F. de Groot, S. Pizzini, A. Fontaine, K. Hämäläinen, C.-C. Kao, and J. B. Hastings, Phys. Rev. B **51**, 1045 (1995).
[11] G. Peng, F. M. F. de Groot, K. Hämäläinen, J. A. Moore, X. Wang, M. M. Grush, J. B. Hastings, D. P. Siddons, W. H. Armstrong, O. C. Mullins, and S. P. Cramer, J. Am. Chem. Soc. **116**, 2914 (1994).
[12] X. Wang, F. M. F. de Groot, and S. P. Cramer, Phys. Rev. B **56**, 4553 (1997).
[13] V. I. Anisimov, J. Zaanen, and O. K. Andersen, Phys. Rev. B **44**, 943 (1991).
[14] A. Georges, G. Kotliar, W. Krauth, and M. J. Rozenberg, Rev. Mod. Phys. **68**, 13 (1996).
[15] V. I. Anisimov, *Strong Correlations in Electronic Structure Calculations* (Gordon and Breach, Amsterdam, 2000).
[16] S. Satpathy, Z. S. Popovic, and F. R. Vukajlovic, Phys. Rev. Lett. **76**, 960 (1996).
[17] S. Y. Savrasov, Phys. Rev. B **54**, 16 470 (1996).
[18] J. Rodriguez-Carvajal, M. Hennion, F. Moussa, A. H. Moudden, L. Pinsard, and A. Revcolevschi, Phys. Rev. B **57**, R3189 (1998).
[19] K. R. Poeppelmeier, M. E. Leonowicz, J. C. Scanlon, J. M. Longo, and W. B. Yelon, J. Solid State Chem. **45**, 71 (1982).
[20] G. Peng, F. M. F. de Groot, K. Hämäläinen, J. A. Moore, X. Wang, M. M. Grush, J. B. Hastings, D. P. Siddons, W. H. Armstrong, O. C. Mullins, and S. P. Cramer, J. Am. Chem. Soc. **116**, 2914 (1994).
[21] X. Wang, F. M. F. de Groot, and S. P. Cramer, Phys. Rev. B **56**, 4553 (1997).
[22] F. M. F. de Groot, A. Fontaine, C.-C. Kao, and M. Krisch, J. Phys.: Condens. Matter **6**, 6875 (1994).
[23] K. Tsutsumi, H. Nakamori, and K. Ichikawa, Phys. Rev. B **13**, 929 (1976).
[24] Q. Qian, T. A. Tyson, C.-C. Kao, M. Croft, S.-W. Cheong, G. Popov, and M. Greenblatt, Phys. Rev. B **64**, 024430 (2001).
[25] L. Hozoi, A. H. de Vries, and R. Broer, Phys. Rev. B **64**, 165104 (2001).
[26] S-W Cheong and H. Y. Hwang, in *Colossal Magnetoresistance Oxides*, edited by Y. Tokura (Gordon & Breach, Abingdon, UK, 2000).
[27] M. Takahashi, J.-I. Igarashia, and P. Fulde, J. Phys. Soc. Jpn. **69**, 1614 (2000).
[28] W. E. Pickett and D. J. Singh, Phys. Rev. B **53**, 1146 (1996).
[29] J. B. Goodenough, Phys. Rev. **100**, 564 (1955).
[30] T. Hotta, S. Yunoki, M. Mayr, and E. Dagotto, Phys. Rev. B **60**, 15009 (1999).
[31] S. Satpathy, Z. S. Popovic, F. R. Vukajlovic, J. Appl. Phys. **79**, 4555 (1995).
[32] H. L. Ju, H.-C. Sohn, and K. M. Krishnan, Phys. Rev. Lett. **79**, 3230 (1997).
[33] E. O. Wollan and W. C. Koehler, Phys. Rev. **100**, 545 (1955).
[34] A. Moreo, S. Yunoki, and E. Dagotto, Science **283**, 2034 (1999).
[35] P. G. Radaelli, D. E. Cox, M. Marezio, S-W. Cheong, P. E. Schiffer, and A. P. Ramirez, Phys. Rev. Lett. **75**, 4488 (1995).
[36] J. J. Neumeier and J. L. Cohn, Phys. Rev. B **61**, 14319 (2000).
[37] T. Atou, H. Chiba, K. Ohoyama, Y. Yamaguchi, and Y. Syono, J. Solid State Chem. **145**, 639 (1999), and references therein.
[38] Q. Qian *et al.* (unpublished).
[39] J. Rodriguez-Carvajal, M. Hennion, F. Moussa, A. H. Moudden, L. Pinsard, and A. Revcolevschi, Phys. Rev. B **57**, R3189 (1998).
[40] F. M. F. de Groot, S. Pizzini, A. Fontaine, K. Hämäläinen, C.-C. Kao, and J. B. Hastings, Phys. Rev. B **51**, 1045 (1995).